

Evolutionary Status of Dwarf “Transition” Galaxies

Patricia M. Knezek, Kenneth R. Sembach ¹

Department of Physics and Astronomy, The Johns Hopkins University, Baltimore, MD
21218-2695

Electronic mail: pmk@pha.jhu.edu, sembach@pha.jhu.edu

and

John S. Gallagher III ¹

Department of Astronomy, University of Wisconsin, Madison, WI 53706-1582

Electronic mail: jsg@astro.wisc.edu

Received _____; accepted _____

¹Guest observer at the Michigan-Dartmouth-MIT Observatory

ABSTRACT

We present deep B -band, R -band, and $H\alpha$ imaging of 3 dwarf galaxies: NGC 3377A, NGC 4286, and IC 3475. Based on previous broadband imaging and H I studies, these mixed-morphology galaxies have been proposed to be, respectively, a gas-rich low surface brightness Im dwarf, a nucleated dwarf that has lost most of its gas and is in transition from Im to dS0,N, and the prototypical example of a gas-poor “huge low surface brightness” early-type galaxy (Sandage & Hoffman 1991, Sandage & Binggeli 1984). From the combination of our broadband and $H\alpha$ imaging with the published information on the neutral gas content of these three galaxies, we find that (1) NGC 3377A is a dwarf spiral, similar to those found by Schombert et al. (1995) and Matthews & Gallagher (1997); (2) both NGC 3377A and NGC 4286 have comparable amounts of ongoing star formation, as indicated by their $H\alpha$ emission, while IC 3475 has no detected H II regions to a very low limit; (3) the *global* star formation rates are at least a factor of 20 below that of 30 Doradus for NGC 3377A and NGC 4286; (4) while the amount star formation is comparable, the *distribution* of star forming regions is very different between NGC 3377A and NGC 4286, with $H\alpha$ emission scattered over most of the optical face of NGC 3377A, and all contained within the inner half of the optical disk of NGC 4286; (5) given their current star formation rates and gas contents, *both* NGC 3377A and NGC 4286 can continue to form stars for more than a Hubble time; (6) both NGC 3377A and NGC 4286 have integrated total $B - R$ colors that are redder than the integrated total $B - R$ color for IC 3475, and thus *it is unlikely that either galaxy will ever evolve into an IC 3475 counterpart*; and (7) *IC 3475 is too blue to be a dE*. We thus conclude that we have not identified potential precursors to galaxies such as IC 3475, and unless significant changes

occur in the star formation rates, neither NGC 3377A nor NGC 4286 will evolve into a dwarf elliptical or dwarf spheroidal within a Hubble time. Furthermore, *optical morphology, even when coupled with the knowledge of the neutral gas content of a dwarf galaxy, is not sufficient to determine its evolutionary phase.* The evolutionary states of NGC 3377A and NGC 4286 are thus unclear and more complicated than might be inferred from either previous broad-band imaging or H I content alone.

Subject headings: galaxies: evolution — galaxies: individual (IC 3475, NGC 3377A, NGC 4286) — galaxies: irregular

1. Introduction

An outstanding question in galaxy evolution is whether there is an evolutionary connection between the various morphological classes of dwarf galaxies. One view is that all dwarfs form in a similar manner, and the separation of dwarf irregulars (dSm/dIm) from early type dwarfs (dS0/dEs) takes place at a later evolutionary phase. For example, it has been suggested that dIm systems might evolve into dE or dS0 galaxies after they lose their gas (e.g., Lin & Faber 1983, Thuan 1985). This might occur as a result of supernova driven winds during starbursts (Dekel & Silk 1986, Babul & Rees 1992, De Young & Heckman 1994, Spaans & Norman 1997), or as a result of an external interaction, such as ram pressure stripping (Kormendy 1985, Binggeli 1986) or galaxy collisions (Henriksen & Byrd 1996, Moore et al. 1996, 1998). However, none of these mechanisms is able to reproduce the full range of differences between dIm and dE galaxies seen in the primary surface brightness-luminosity, luminosity-metallicity, and luminosity-rotation velocity correlations (and lack thereof in dEs) (see Silk & Wyse 1993, Hunter & Gallagher 1985, Bothun et al. 1986, Ferguson & Binggeli 1994, Skillman & Bender 1995, Walsh et al. 1997). At the present time we still do not understand the physical origins of the two main families of low luminosity galaxies.

Properties of ‘transition’ dwarf galaxies, systems that show a mixture of early and late-type dwarf galaxy characteristics, therefore continue to be of special interest. Sandage & Hoffman (1991) proposed that the galaxies NGC 3377A, NGC 4286, and IC 3475 present an example of the progression of gas-rich dwarfs (dSm/dIms) to gas-poor dwarfs (dE/dS0s). In a test to determine whether or not dIms could evolve into nucleated dwarf ellipticals, they chose two “missing link” galaxies that had optical evidence from photographic plates of the mixed morphology of an underlying dE or dS0 with current star formation that was distributed globally over the optical surfaces of the galaxies.

The first of these galaxies was NGC 3377A, known to be a gas-rich dwarf with many “knots” over its face. The second galaxy was NGC 4286, which also showed “knots” over its face in a blue image, and a hint of spiral structure in its “outer envelope”. Sandage & Hoffman obtained H I data for NGC 4286 and found that the galaxy is gas-poor, although it still contains a moderate mass of H I. Based on the combination of the optical morphology from photographic plates and the gas content from H I data, they concluded that NGC 4286 is indeed a galaxy in transition from Im to dS0, while NGC 3377A has not yet been transformed. They proposed that NGC 3377A is similar to the giant, very low surface brightness (VLSB) galaxy IC 3475. IC 3475 is a Virgo Cluster galaxy with little atomic gas, and a non-nucleated optical morphology with statistical excess of marginally resolved embedded images over its face (Reaves 1956; Bothun et al. 1986). Its optical light distribution is best fit by an exponential light profile (Vigroux et al. 1986), leading to the suggestion that it is a stripped dwarf irregular. To determine the validity of Sandage & Hoffman’s proposition, we obtained deep broadband B and R CCD images, as well as narrow-band $H\alpha$ images of these three galaxies to accurately determine their underlying stellar distribution and their current star formation rates (SFRs).

In §2 we discuss the observations and reduction. In §3 we discuss each galaxy individually and intercompare them. We also discuss the results in light of the picture proposed by Sandage & Hoffman (1991). §4 contains our conclusions.

2. Observations and Data Reduction

2.1. Observations

Direct imaging observations were made at Michigan-Dartmouth-MIT Observatory on the 1.3 m McGraw–Hill telescope. The data were taken on 10 - 12 April 1996 with a

1024x1024 thinned CCD. The pixel scale is $\sim 0.50''/\text{pix}$ for this detector and telescope with the $f/7.5$ secondary, giving a field of view of $\sim 8'.5 \times 8'.5$. Broadband B and R images were made using the MDM Schombert filter set. These filters closely approximate the wavelength coverage of the Kitt Peak National Observatory “Harris Set” of broadband filters, although the transmission efficiencies are lower. Narrowband $H\alpha$ imaging was done using a set of extragalactic $H\alpha$ interference filters on loan from Deidre Hunter. For NGC 3377A and NGC 4286, a filter centered at $\sim \lambda 6590\text{\AA}$ was used. For IC 3475, a filter centered at $\sim \lambda 6612\text{\AA}$ was used. Both filters have a FWHM of $\sim 30\text{\AA}$, and thus only include $H\alpha$ emission. Typical integrations times were 20-30 minutes in B , 10-15 minutes in R , and 40-60 minutes in $H\alpha$. Several Landolt standard fields (Landolt 1992) were observed each night in the broadband filters, and the spectroscopic standard Feige 34 was observed in R and each $H\alpha$ filter. The atmospheric extinction was determined using the Landolt standards and found to be consistent with the standard Kitt Peak extinction coefficients.

2.2. Data Reduction

Initial data processing was done using the CCD reduction tasks in IRAF². The data were overscan-subtracted, and then bias subtracted using a median filtered bias from each night. Primary flat fielding was done using sky flats obtained each evening. After applying the sky flats typical variations were 1% in B , 1.5% in R , and 3% in the two $H\alpha$ filters. These variations do not include the corners of the images, where there was vignetting that was apparently due to slight fluctuations in the filter wheel stopping point. In no case

²IRAF is distributed by the National Optical Astronomy Observatories, which are operated by the Association of Universities for Research in Astronomy, Inc., under contract to the National Science Foundation.

does the vignetting affect the portion of the image including the galaxies, and the regions affected have been excluded from the remaining analysis. When there were three or more individual exposures for a galaxy in one band, the exposures in each band were aligned and then combined using a median filter with no rejection. Any residual cosmic rays were removed by hand. For cases when there were only one or two exposures of a galaxy in a band, cosmic rays were removed with the task *COSMICRAYS* in IRAF, with any residual cosmic rays removed by hand. If there were two exposures, they were aligned and then combined by averaging with no rejection. Sky values for the final images were determined by taking the average of ~ 15 sky boxes around the images in regions selected to be free from galaxy emission, stars, bad pixels, and vignetting. The box size was typically 15 pixels on a side. The sky value was then subtracted from the final images during the determination of the magnitudes and the radial surface brightness profiles of the galaxies.

In order to obtain the $H\alpha$ flux for each galaxy, the observations of the spectrophotometric standard Feige 34 were used. Feige 34 was observed under photometric conditions in both the R and $H\alpha$ filters. The transmission curve of each filter was convolved with the quantum efficiency of the CCD detector. The resulting curve was then multiplied by the atmospheric extinction curve. (The KPNO extinction curve was used for this step, given that our broadband photometry implied that the extinction during our run was consistent with it.) The spectral energy distributions of Feige 34 and BD+17°4708 were then convolved with the corrected efficiency curve, and the magnitude of BD+17°4708 was set to 9.500 in each filter in order to place the magnitudes on the AB_ν system of Oke & Gunn (1983). The magnitude of Feige 34 in each filter was then calculated relative to BD+17°4708, and the relationship between the magnitude in each filter and the AB_ν magnitude was found using the relationship of Windhorst et al. (1991):

$$AB_\nu = AB_\nu(\text{BD} + 17^\circ 4708) + m_\lambda(\text{filter}) - m_\lambda(\text{BD} + 17^\circ 4708)$$

where “filter” is either the R filter or one of the $H\alpha$ filters, and $AB_\nu(\text{BD}+17^\circ 4708)$ is calculated at the appropriate wavelength from Oke & Gunn (1983). Using these magnitudes and the measured instrumental magnitudes, a zero point was determined for each filter separately using the relationship:

$$AB_\nu = (m_{\text{inst}} - k_\nu * X_\nu) + \zeta$$

The actual flux values could then be determined using the relationship of Windhorst et al. (1991):

$$AB(\text{filter}) = -2.5 \log F_\nu / d\nu \text{ (ergs cm}^{-2} \text{ s}^{-1}) + 48.594$$

The total integrated $H\alpha$ magnitudes were measured at different points within each galaxy. For the two galaxies with positive detections of $H\alpha$ emission, NGC 3377A and NGC 4286, the radius was chosen such that it included all of the $H\alpha$ emission visible in the image and avoided poorly subtracted stars. (In the case of NGC 3377A, one poorly subtracted star is included, which introduces an uncertainty of $\sim 10\%$ to the determined flux.) For IC 3475, the reported upper limit was calculated at a radius of $75''$ by taking three times the reported counts within the aperture and converting that to an apparent magnitude.

3. Discussion

Our research was inspired by the suggestion by Sandage & Hoffman (1991) that the galaxies NGC 3377A, NGC 4286, and IC 3475 present examples of an evolutionary sequence running from typical gas-rich late-type dwarfs (dSm/dIms) to gas-poor dwarfs (dE/dS0s). We obtained broadband B and R imaging, along with $H\alpha$ imaging in order to compare the underlying stellar population, and ongoing star formation (if any), with published neutral gas properties.

Table 1 lists the cataloged properties of the 3 galaxies in this study. Column 1 lists the galaxy name. Columns 2 and 3 list the right ascension and declination in J2000.0 coordinates. Column 4 lists the heliocentric velocity in km s^{-1} . Columns 5 and 6 list the major and minor axes in arcminutes. Column 7 lists the total B magnitude. Column 8 lists the H I flux in Jy km s^{-1} . Column 9 lists the morphological type. All properties except the H I flux were obtained from the NASA/IPAC Extragalactic Database³. The H I measurements are from Schneider et al. (1990) for NGC 3377A, Sandage & Hoffman (1991) for NGC 4286, and Huchtmeier & Richter (1986) for IC 3475.

Table 2 presents the results of our photometry. Column 1 lists the galaxy name. Columns 2 and 3 list the total integrated magnitudes and magnitude errors of the galaxies in the B and R bands, respectively. These magnitudes were derived through circular aperture photometry, and have not been corrected for contributions from foreground stars or for Galactic or internal extinction. Column 4 lists the total integrated magnitude of the $\text{H}\alpha$ emission after subtracting off the continuum. In the case of IC 3475, the reported $\text{H}\alpha$ magnitude is a 3σ lower limit. Because only one spectrophotometric standard was observed, the errors on the $\text{H}\alpha$ magnitudes are uncertain. However, the spectroscopically determined R band flux for Feige 34 agrees to within $\sim 30\%$ of the broadband flux calculated using the Landolt (1992) standards, so we estimate that our $\text{H}\alpha$ measurements are also accurate to $\sim 30\%$. We have included an additional 10% uncertainty for NGC 3377A due to the imperfectly subtracted star. Column 5 lists the total integrated $B - R$ color and its error at the last measured point for each galaxy, except for IC 3475. For IC 3475 the light

³The NASA/IPAC Extragalactic Database (NED) is operated by the Jet Propulsion Laboratory, California Institute of Technology, under contract with the National Aeronautics and Space Administration.

distribution is very flat and close to the sky level in the outer regions, and the colors are dominated by possible systematic errors in the sky level. Thus we have chosen to quote the color within $65''$ of the center, which is well within the region where the galaxy light still dominates. The color is consistent with the color at the last measured point. The errors quoted for the magnitudes and colors do not include possible systematic effects. Column 6 lists the diameter of the galaxy at the B_{25} mag arcsec $^{-2}$ isophote (corrected for Galactic extinction). Column 7 lists the color excess due to Galactic extinction, $E(B - V)$. This color excess was derived using the standard dust-to-gas ratio given by Diplás & Savage (1994),

$$E(B - V) = \frac{4.93 \times 10^{21}}{N(HI)}$$

where $N(HI)$ was determined by integrating the H I 21 cm emission profile toward each galaxy as observed in the Leiden-Dwingeloo H I Survey (Hartmann & Burton 1997).

Table 3 lists the derived optical and neutral gas properties of the 3 galaxies in this study. Column 1 lists the galaxy name. Column 2 lists the distances, which were adopted from Tonry et al. (1997) for NGC 3377A and NGC 4286, and from Garcia et al. (1996) for IC 3475. Columns 3 and 4 list the absolute B and R magnitudes, respectively, based on magnitudes corrected for Galactic extinction. No correction has been applied for internal extinction. Column 5 lists the $H\alpha$ luminosity. All the optical data is based on our broadband and $H\alpha$ imaging. Column 6 lists the H I masses, which were calculated using the fluxes from Table 1, the adopted distances, and the relation $M_{HI} = 2.36 \times 10^5 D^2 S_{HI} M_{\odot}$. Column 7 lists the H_2 mass for NGC 4286, from Gerin & Casoli (1994), scaled to our adopted distance. Column 8 is a measure of the ratio of atomic gas to light, M_{HI}/L_B , where we have adopted $M_B(\text{Sun}) = +5.48$. Column 9 lists the current star formation rate calculated following the prescription of Kennicutt et al. (1994), who rederived the

relationship using the models of Schaller et al. (1993). We have adopted a Salpeter Initial Mass Function. The star formation rate is then (see Kennicutt et al. 1994, Table 2):

$$\text{SFR} = 1.26 \times 10^{-41} L(\text{H}\alpha) M_{\odot} \text{ yr}^{-1}$$

Column 10 indicates the amount of time that star formation can continue at the current level, estimated by dividing the current star formation rate by the available gas content. In this case, we have chosen to use the H I mass for the estimate, since the H₂ content has only been measured in one galaxy, and the CO-H₂ conversion rate is uncertain. This calculation assumes that the entire H I mass is available for use in star formation, and we have multiplied by a factor of 1.4 to include helium and the heavy elements.

3.1. NGC 3377A

NGC 3377A is located in the Leo I (M 96) group, and it is thought to be a companion to the E6 elliptical NGC 3377. Its projected distance is only ~ 22 kpc from NGC 3377. It is gas-rich, $M_{HI}/L_B \sim 0.30$. In the B image, which can be seen in Figure 1a, its outer optical morphology is actually that of a late-type spiral, similar to the ‘extreme late-type’ dwarf spirals. Figure 1b, which is a composite image of the B band (represented as blue), R band (represented as red), and continuum subtracted H α (represented by green), shows that it has a number of regions of active star formation spread over almost the entire optical area of the galaxy, as well as regions of diffuse H α emission. The bright object near the “center” is either a foreground star or a star cluster with colors comparable to the underlying stellar population. There is no detected H α emission, so it is *not* an H II region sinking to the center as suggested by Sandage & Hoffman (1991).

The radial surface brightness distribution of NGC 3377A was determined within

concentric circular annuli from a somewhat arbitrarily chosen center. The center was selected to be as close to the “center” of the underlying central stellar distribution in R as possible by looking at the outer R isophotes. It lies approximately halfway between the bright stellar-like central region and a more diffuse light concentration of light (both free of $H\alpha$ emission) approximately $10''$ southwest (see Figure 1). This diffuse light concentration may be the dynamical center of the galaxy, or simply a large star cluster. In either case, it is slightly off-center in the R band, and thus was not used as the center in this analysis. The interactively determined center was then used to fit the magnitudes and surface brightness distributions in B , R , and $H\alpha$. The radial $B - R$ colors were determined both by subtracting the integrated R magnitude from the integrated B magnitude at the same radius, and by subtracting the R magnitude determined within an annulus from the B magnitude within the same annulus.

Figure 2a shows the radial distributions for NGC 3377A. The top panel contains the surface brightness distributions in B (squares), R (circles), and $H\alpha$ (diamonds) as a function of radius. A typical error bar for the B and R surface brightness distributions is shown in the upper right portion of the top panel. Errors in the $H\alpha$ distribution are dominated by the uncertainty in the flux zero point, and are estimated to be $\sim 30\%$. Our calculated $B_T = 14.20 \pm 0.05$ agrees well with de Vaucouleurs et al. (1991, hereafter RC3), who find $B_T = 14.22$. The B surface brightness distribution decreases by ~ 1.5 magnitudes arcsec^{-2} from the center to $\sim 90''$. The dashed lines show simple linear fits to the data using only points at $r > 60''$ for B and R . This galaxy is fit very well in the outer regions in both bands by the linear relationship, but there is evidence of some excess light in the center. The origin of this excess light is unclear strictly from the optical images. It is not apparent that there is any “spheroidal” component in this galaxy, nor is there clear evidence for an optical bar, as is seen in IC 3475 (Vigroux et al. 1986 and this paper). This may be a case similar to those found by Matthews & Gallagher (1997) where there is a surface brightness

“step” in the disk. Knezek (1993) also found that many objects in her sample of more massive disk galaxies required the fit of a second “disk” component, independent of the presence of a well-fit bulge component, in order to fully model the light distribution. The coefficients of the fit to the outer $60''$ are listed in Table 4. Column 1 lists the galaxy name. Column 2 lists the filter. Column 3 lists the central surface brightness in mag arcsec^{-2} . Columns 3 and 4 list the disk scale length in arcsec and kpc, respectively. This disk scale length was derived using the relationship (de Vaucouleurs 1959):

$$\mu = \mu_0 + \frac{r}{\alpha}.$$

The $H\alpha$ distribution, which was measured in concentric annuli, decreases overall as a function of radius, but with some structure. This non-linear distribution reflects the “lumpy” nature of the $H\alpha$ emission over the surface of the galaxy. The global amount of $H\alpha$ emission is relatively low, $L_{H\alpha} \sim 2.6 \times 10^{38} \text{ erg s}^{-1}$, where the $H\alpha$ luminosity of 30 Doradus is $\sim 5 - 10 \times 10^{39} \text{ erg s}^{-1}$ (Kennicutt & Hodge 1986). In fact, most of the quiescent dwarfs galaxies studied by van Zee et al. (1997a) have more $H\alpha$ luminosity (although there are some systems with comparable amounts). In particular, for those galaxies of van Zee et al. (1997a) that are classified as dwarf spirals, most have ~ 10 times more global $H\alpha$ emission. Thus NGC 3377A appears to be a very quiescent dwarf spiral, despite its dense environment, and in this sense represents a true transition object between low SFR dE and normal late-type dwarf galaxies.

The middle and bottom panels of Figure 2a show the integrated $B - R$ color and annular $B - R$ color as a function of radius, respectively. NGC 3377A is blue over its entire optical disk, and becomes bluer with increasing radius. In the central region, its integrated $B - R$ is ~ 1.05 , decreasing to ~ 0.90 in the outer regions of the disk. The integrated and annular colors for this galaxy are very similar over the radial extent for which we are able

to reliably measure the annular colors. Both the integrated and annular colors show a fairly steep blueing ($\Delta(B - R) \sim 0.1 - 0.2$) from the center out to $\sim 30''$, then approximately level off, again indicating the possibility of two disk components. Furthermore, as can be seen in the bottom panel of Figure 2a, there is evidence that this second component is actually slightly *redder* than the inner disk component. Reddening in outer disks was also seen in some dwarf spirals in the sample of Matthews & Gallagher (1997). For the disks of spiral galaxies, Bothun et al. (1985) found that the average $B - R$ color is 1.25. Thus, NGC 3377A is bluer *at all points* than the typical spiral galaxy disk. The mean colors, however, are not abnormally blue for dwarf and low surface brightness galaxies (Gallagher & Hunter 1986, Knezek 1993, Schombert et al. 1990, McGaugh & Bothun 1994, de Blok et al. 1995, van Zee et al. 1996, van Zee et al. 1997a, van Zee et al. 1997b). The colors are blue enough, however, that if most of the stellar population is comparable in age to globular clusters around the Milky Way, it must be very metal poor. Reed (1985) found that low metallicity Milky Way globular clusters have mean colors, $\langle B - R \rangle = 1.16$, *redder* than the colors of NGC 3377A at all points. It seems unlikely, however, given the presence of active star formation within its disk, that the colors are due only to a very metal-poor old stellar population.

Despite its location in a dense environment, NGC 3377A resembles the dwarf spirals studied by Matthews & Gallagher (1997) and Schombert et al. (1995) in terms of optical structure, H I content, stellar luminosity, and colors. In fact, NGC 3377A appears to be a fairly “typical” dwarf spiral in H I gas mass, mass-to-light ratio, optical morphology, and colors. It also resembles the gas-rich quiescent dwarfs recently examined by van Zee et al. (1997a) (many of which are also classified as dwarf spirals), although it is bluer. (van Zee et al. find $B - R$ colors for their sample of galaxies that are on average the same as those of Bothun et al. 1985 for spiral disks.) As can be seen in Table 3, NGC 3377A has a very low SFR ($\sim 0.0033 M_{\odot} \text{ yr}^{-1}$). We have used a different prescription than van Zee et al. (1997a) to derive the SFR, but it should be noted that our prescription implies a *higher*

SFR than that of van Zee et al. Even so, our derived SFR is on the low end of those found by van Zee et al., and it is at least a factor of 10 lower than those of the galaxies classified as dwarf spirals in their sample. The length of time that NGC 3377A can continue to form stars at the current rate, however, is comparable, and much longer than a Hubble time. Thus, unless it is significantly affected by its environment in the future, NGC 3377A is not going to evolve into a dE anytime soon. Furthermore, it is unlikely to evolve into a galaxy like IC 3475, as its total integrated color within the detected broadband emission, $(B - R) \sim 1.15$ (corrected for Galactic extinction and with foreground stars masked) is already *redder* than IC 3475 ($(B - R) \sim 1.10$).

3.2. NGC 4286

NGC 4286 is a member of the Coma I group, at a projected distance of ~ 36 kpc from the E1 galaxy NGC 4278, a H I-rich elliptical. It is gas-poor, $M_{HI}/L_B \sim 0.03$, with a broadband optical mixed morphology between a late-type dwarf and a dwarf elliptical or dwarf spheroidal. Figure 1c is the B band image of this galaxy, which has been stretched to emphasize the faint spiral-like structure noted by Sandage & Hoffman (1991) in the inner part of the disk, where all the current star formation is occurring. The outer regions of the galaxy, however, are quite smooth and featureless, giving rise to the “transition” dS0 morphological characteristics. Unlike NGC 3377A and IC 3475, this galaxy is inclined. This is confirmed not just from the optical appearance of the outer isophotes (Figure 1c), but also from the fact that unlike NGC 3377A and IC 3475, the H I emission is double-horned (Sandage & Hoffman 1991). Figure 1d, which is a composite image of the B band (represented as blue), R band (represented as red), and continuum subtracted $H\alpha$ (represented by green), shows that the galaxy also has a number of active regions of star formation. The emission is more centrally concentrated than for NGC 3377A. Nearly all the

detected H α emission for NGC 4286 lies within $\sim 40''$, which is ~ 3 kpc. The *total* extent of the H α emission of NGC 3377A is comparable, lying within $\sim 75''$, which corresponds to ~ 4 kpc. However, since NGC 4286 is so much larger ($D(B_{25}) \sim 7.3$ kpc for NGC 4286 versus ~ 4.6 kpc for NGC 3377A), the relative concentration is very different. This is also seen in the upper panels of Figures 2a and 2b, where the radial distribution of H α is only slowly falling with radius for NGC 3377A, but the radial distribution of H α drops sharply for NGC 4286. The bright object near the center *is* an H II region that may have sunk to the center, as suggested by Sandage & Hoffman (1991). NGC 4286 has tentatively been detected in ^{12}CO (Gerin & Casoli 1994), and the implied molecular-to-atomic gas ratio is $M_{H_2}/M_{HI} \sim 0.23$ (assuming a galactic conversion factor between ^{12}CO and H_2 , Strong et al. 1988). This is comparable to ratios found in late-type disk galaxies (Young & Knezek 1989). Early-type disk galaxies have much higher ratios. This ratio suggests that if NGC 4286 is a galaxy in transition, it has lost much of its gas, not converted it into molecular hydrogen. Even if NGC 4286 is as metal-poor as local dwarf irregulars such as IC 10 and NGC 6822, the increase in the molecular-to-atomic gas ratio is likely to be at most a factor of 3 (Wilson 1995). Then the *total* gas mass-to-light ratio is $M_{gas}/L_B \sim 0.05$, and NGC 4286 is still a gas-poor galaxy.

Figure 2b shows the radial surface brightness distribution of NGC 4286 along the major axis. The position angle was taken from RC3. The top panel contains the surface brightness distributions in B (squares), R (circles), and H α (diamonds) as a function of radius. The center was determined within concentric circular annuli from the central peak of the underlying central stellar distribution in R , which corresponds to an H II region. A typical error bar for the B and R surface brightness distributions is shown in the upper right portion of the top panel. Errors in the H α distribution are dominated by the uncertainty in the flux zero point, and are estimated to be $\sim 30\%$. The same center was then used to fit the magnitudes and surface brightness distributions in B , R , and H α . No B_T was

listed in RC3 to compare to our value of $B_T = 13.71 \pm 0.05$. The radial $B - R$ colors were determined both by subtracting the integrated R magnitude within a radius from the integrated B magnitude within the same radius (middle panel of Figure 2b), and by subtracting the R magnitude determined within an annulus from the B magnitude within the same annulus (bottom panel of Figure 2b). As a check, the radial distributions were also calculated independently within concentric boxes of 10 by 10 pixels along the major and minor axes. No significant differences in the shapes of the radial distributions of stellar light, $H\alpha$ luminosity, or the color gradients were seen between the two axes.

As can be seen in the upper panel of Figure 2b, the radial surface brightness distribution for NGC 4286 deviates significantly from a simple exponential disk. Unlike NGC 3377A and IC 3475 (upper panels of Figures 2a and 2c, respectively), which show only small deviations, NGC 4286 requires a significant secondary component. In fact, it appears that the secondary component dominates out to at least $60''$, which is $0.6 D(B_{25})$ (see below). To illustrate this point, we show the overlay of a simple linear regression analysis on radii $\gtrsim 60''$ of the B and R images as a function of radius. Again, this characteristic is also found in some extreme late-type spirals (Matthews & Gallagher 1997). The coefficients of the fit to the outer $60''$ are listed in Table 3. The $H\alpha$ surface brightness distribution increases from $5''$ to $10''$ despite the fact that there is an H II region at the center. This may be due partly to internal extinction. Outside of $10''$ the surface brightness decreases smoothly. It is interesting to note that, unlike NGC 3377A, *all* of the $H\alpha$ emission detected in NGC 4286 lies within the inner “secondary component”, and thus much of this inner light distribution, which is also bluer than the outer regions of the galaxy (see below), may be due to the star formation.

From the middle and lower panels of Figures 2a and 2b, we can see that like NGC 3377A, NGC 4286 is blue over its entire optical disk. The two galaxies have similar

annular $B - R$ colors in their inner $10''$ ($(B - R)_{ann} \sim 1.05$). Except in the innermost point (which may be due simply to the fact that NGC 4286 center is an H II region), the integrated and annular colors follow similar radial trends. However, while NGC 3377A becomes bluer with increasing radius, before levelling out at $\sim 30''$, NGC 4286 is nearly constant within the inner $15''$ and becomes slightly redder with increasing radius, increasing to $(B - R)_{ann} \sim 1.15$ at $40''$. The integrated $B - R$ colors also become redder until $\sim 40''$, then remain approximately constant, $(B - R)_{int} \sim 1.10$, within $D(B_{25}) = 98''$. There is no evidence of any difference between the major and minor axes within the errors. The inner $40''$ is also the region where most of the $H\alpha$ emission occurs, which is consistent with the blue colors. Including a correction for internal extinction - most of which presumably is in the center of the galaxy where the H II regions are - would only enhance the difference in colors between the inner and outer regions. The annular disk colors at greater than $40''$ (outside the regions of active ongoing star formation) are comparable to the colors of IC 3475 at a comparable radius, while the annular colors of NGC 3377A are bluer *over the entire optical face* (see the bottom panels of Figures 2a-c). This suggests that at least some regions of the disks of NGC 4286 and IC 3475 have older underlying stellar populations and/or significant chemical enrichment compared to NGC 3377A. Again, based on the study of low metallicity globular clusters by Reed (1985), if the outer disk populations are old, they are very metal poor. However, while the integrated colors of NGC 4286 truly level off to $(B - R)_{int} \sim 1.10$ out towards the edge of the detected optical disk, and perhaps even redden slightly ($(B - R)_{int} \sim 1.26$ at the outermost measured point), the integrated colors of IC 3475 appear to get bluer with radius, and already have $(B - R)_{int} \sim 1.10$ within $65''$. Thus, NGC 4286 is *already too red* to fade into a galaxy like IC 3475. Furthermore, its SFR is comparable to that of NGC 3377A, $\sim 0.0034 M_{\odot} \text{ yr}^{-1}$, again on the low end of even the quiescent dwarfs studied by van Zee et al. (1997a). *Despite the fact that NGC 4286 is gas poor, assuming all of its gas is available to form stars, it can continue to form stars at its*

present level for more than a Hubble time.

3.3. IC 3475

Garcia et al. (1996) derive a distance of 14.2 Mpc for IC 3475 and two ellipticals located nearby at about the same velocity, NGC 4168 (E2) and NGC 4473 (E6), which would place them in front of the Virgo Cluster ($D = 17$ Mpc, Kennicutt et al. 1995). However, even if IC 3475 is not actually located near the center of Virgo (projected distance ~ 170 kpc from the Virgo Cluster core, at the distance of M 100), it appears to be in a dense environment with nearby elliptical galaxies, similar to NGC 3377A and NGC 4286. Like NGC 4286, it is also gas-poor, $M_{HI}/L_B < 0.09$, with a fairly smooth, diffuse morphology characteristic of a dwarf elliptical or a dS0. Since it is not significantly centrally concentrated, its classification is closer to dS0 than dE (c.f. Ferguson & Binggeli 1994). Figure 1e is the B band image of this galaxy, which has been stretched to emphasize the faint bar-like structure in the central region, which was noted by Vigroux et al. (1986). Figure 1f, which is a composite image of the B band (represented as blue), R band (represented as red), and continuum subtracted $H\alpha$ (represented by green), shows that there is no evidence of any $H\alpha$ emission at a 3σ flux level of $f_\nu = 5.15 \times 10^{-14}$ ergs cm^{-2} s^{-1} within a radius of $75''$ from the “center”. Also, as found by Vigroux et al. (1986), none of the “bumps” have anomalously blue colors. Furthermore, if IC 3475 had any H II regions with emission comparable to the fainter H II regions in NGC 3377A or NGC 4286, they would have been detectable with our data. The 3σ detection limit for a potential H II region in IC 3475, scaled in size by the difference in distances, is almost a factor of 2 below the flux detected in a comparable faint H II region in NGC 3377A. Thus, this galaxy does not appear to have any significant ongoing star formation, nor does there appear to have been any star formation in the recent past.

Figure 2c shows the radial distributions for IC 3475. The top panel contains the surface

brightness distributions in B (squares), R (circles), and $H\alpha$ (diamonds) as a function of radius. A typical error bar for the B and R surface brightness distributions is shown in the upper right portion of the top panel. Errors in the $H\alpha$ distribution are dominated by the uncertainty in the flux zero point, and are estimated to be $\sim 30\%$. The radial surface brightness distribution of IC 3475 was determined within concentric circular annuli from a somewhat arbitrarily chosen center. The center was selected to be as close to the “center” of the underlying central stellar distribution in R as possible by looking at the outer R isophotes and the central bar-like structure. The same center was then used to fit the magnitudes and surface brightness distributions in B , R , and $H\alpha$. The radial $B - R$ colors were determined both by subtracting the integrated R magnitude within a radius from the integrated B magnitude within the same radius (middle panel of Figure 2c), and the R magnitude determined within an annulus from the B magnitude within the same annulus (bottom panel of Figure 2c). The error bars probably *underestimate* the error in the colors outside of a radius of $\sim 120''$. In the R -band, where the sky is much brighter, we find that outside $\sim 120''$ a change of 1 count/pixel in the sky (which is the standard deviation of the mean of the sky in this image) can produce a ~ 0.1 mag variation in the total magnitude. Thus, we have chosen to be conservative and will only use colors within $65''$, where the variation is seen to be $\lesssim 0.05$ mag.

Our calculated B magnitude, $B_T = 13.95 \pm 0.05$, is a magnitude brighter than that reported by Vigroux et al. (1986, $B_T = 14.7$), but close to the RC3 value, $B_T = 13.82$. However, our determined *central* surface brightness, $\mu_0(B) = 23.65$, agrees well with the value measured by Vigroux et al., $\mu_0(B) = 23.60$. Vigroux et al. (1986) pointed out that IC 3475 nearly filled their field of view, and that their sky background may have been incorrectly subtracted. This also leads to significant differences in the radial surface brightness distributions between our study and theirs. In contrast to Vigroux et al. (1986), who find a decrease of almost 3.5 magnitudes arcsec^{-2} between the center and their last

measured point at $\sqrt{ab} \sim 70''$, we see a decrease of $\lesssim 1.5$ magnitudes arcsec^{-2} over the same radius, again consistent with a sky subtraction difficulty in the previous data. This difference is unlikely to be due to the isophotal photometry methods used (circular apertures in this study, elliptical apertures in the Vigroux et al. (1986) study) since IC 3475 has a small ellipticity (typically $e \lesssim 0.25$, Vigroux et al. (1986)). As can be seen in the upper panel of Figure 2c, IC 3475 has an exponential surface brightness distribution in both B and R , but with a small excess in the inner regions. This deviation from linearity may well be due to the presence of the bar described by Vigroux et al. (1986). The coefficients of the fit to the outer $60''$ are listed in Table 3. The excess light component appears to be similar to that seen in NGC 3377A, and much less extreme than the deviation seen in NGC 4286 (see the upper panels of Figures 2a and 2b).

The middle and lower panels of Figure 2c indicate that both the integrated and annular $B - R$ colors of IC 3475 are only slightly bluer than the disk of a typical spiral galaxy in its inner regions ($(B - R) \sim 1.15 - 1.2$, $r \lesssim 30''$). The integrated colors decrease very slowly to a $(B - R)_{int} \sim 1.10$ out to a radius of $r \sim 65''$, while the annular colors have dropped to $(B - R)_{ann} \sim 1.0$ within the same radius. Given the lack of gas or ongoing star formation, along with the $B - R$ colors, it appears that IC 3475 has completed its last episode of star formation and is now fading. As noted in the section above, its annular colors are comparable to the outer disk of NGC 4286, and only in the outermost areas do they resemble those of NGC 3377A. The inner regions ($\sim 40''$) have colors which are comparable to those of the low metallicity globular clusters (Reed 1985), while the outer regions are bluer and imply that if the stellar population is old and fading, it must be quite metal-poor.

The suggestion that IC 3475 is not a “typical” dE galaxy is further strengthened by its comparison to the sample of dEs studied by Secker et al. (1997) in the Coma Cluster. They found a very tight correlation between the total R magnitude of the Coma dEs and

their $B - R$ colors (see their Figure 4). Even without correcting for Galactic or internal extinction, IC 3475 has an R magnitude of 12.83 ± 0.05 , which corresponds to an apparent magnitude of $R \sim 16.89$ at the distance of Coma, and a $B - R$ color of 1.10 ± 0.04 (see Table 2). Assuming that the $B - R$ color is distance independent, and using the relationship they give in their equation 5 between R magnitude and $B - R$ color, IC 3475 is ~ 0.4 magnitudes *too blue* to be a dE.

3.4. Evolutionary Progression and Environmental Effects

Our data are only partially consistent with the hypothesis proposed by Sandage & Hoffman (1991) that NGC 3377A, NGC 4286, and IC 3475 represent dwarf galaxies in various stages of transition from late to early-types. NGC 3377A appears to be a comparatively normal extreme late-type spiral, while in NGC 4286 the star formation has become centrally concentrated within the stellar disk. As a result the *outer* regions of NGC 4286 now resemble those of a dS0 galaxy, but, its integrated color is already *too red* for it to fade into a galaxy resembling IC 3475 ($B - R \sim 1.10$). IC 3475 appears to be a dE/dS0 in which no recent star formation has occurred. Its position on a $(B - R)$ - R color-magnitude diagram (Secker et al. 1997) is inconsistent with classification as a “typical” dE. What is not clear is whether these galaxies are currently experiencing abnormal evolution towards earlier structural types. The gas reservoirs in both NGC 3377A and NGC 4286 are adequate to sustain their current characteristics for long times. We see no evidence for rapid evolutionary transitions of NGC 4286 or NGC 3377A. If NGC 4286 is a dwarf galaxy “in transition”, as is indicated by its gas-poor nature and its regular outer isophotes, it will *never* fade into a dwarf “stellar fossil” galaxy like IC 3475, although the possibility exists in terms of $B - R$ colors for NGC 4286 to have the *normal* colors of a dE or dS0 galaxy if star formation were to cease.

The effects of environment on the evolution of small galaxies remains relatively poorly understood. Researchers have proposed that the evolution of dwarf galaxies may be driven by internal mass loss due to stellar winds (Sandage 1965; Searle & Zinn 1978; Faber & Lin 1983; Wirth & Gallagher 1984; Matteucci & Chiosi 1983; Matteucci & Tosi 1985; Pilyugin 1992, 1993; Marconi et al. 1994) or by the loss of gas due to stripping in a group or cluster environment (Lin & Faber 1983). However, the picture is not a simple one because the gas distribution, and presumably the subsequent star formation history and stellar light distribution, can be driven by the *type* of environmental interactions, and their significance as compared with internal processes.

Galaxies, particularly dwarf galaxies, in groups and clusters are subject to a variety of environmental influences. The presence of hot intergalactic gas could lead to stripping, especially from the low density outer regions of dwarfs (e.g., Gallagher & Hunter 1989), but the intra-group gas could also cool and accrete, thereby rejuvenating previously moribund dwarfs (Silk et al. 1987). Gravitational interactions between dwarfs and giants will dynamically heat the stars in the dwarfs and can also raise substantial tides (McGlynn & Borne 1991, Gruendl et al. 1993, Valluri 1993, Oh et al. 1995, Moore et al. 1998). When interactions are strong or occur repeatedly, profound changes in the internal mass distributions of dwarfs can occur, including complete disruption (e.g., Séguin & Dupraz 1996). Close passages near gas-rich giants can also lead to gas stripping from a smaller galaxy (Sofue 1994). Other, less intense collisions can redistribute gas, either to be lost into tidal streams (e.g., Gardiner & Noguchi 1996) or to lose angular momentum and drop into the center of the dwarf (e.g., Noguchi 1988).

A variety of intra-group interactions are therefore capable of converting a dwarf galaxy from a gas-rich to a gas-poor state. However, relatively strong interactions are required to change a rotationally supported stellar disk of a Magellanic or extreme late-type spiral

galaxy, which has a ratio of stellar rotation to dispersion velocity that is considerably larger than 1, into a non-rotating dE system where this ratio is <1 (Bender & Nieto 1990, Moore et al. 1998). Transition dwarfs that are not directly involved in strong interactions are therefore likely to be evolving towards gas-poor disk galaxies, or dS0 systems.

Modeling of galaxy interactions indicates that whether gas is stripped from a system or driven to the center of the galaxy can be a sensitive function of the location of the galaxy relative to other systems. NGC 3377A is a dwarf companion to the E6 galaxy NGC 3377, at a projected distance of only ~ 22 kpc (Sandage & Hoffman 1991). NGC 4286 is also a dwarf companion galaxy, in this case to the giant H I-rich elliptical NGC 4278, with a projected linear separation of only ~ 36 kpc (Sandage & Hoffman 1991). The possibility therefore exists that the unusual structure of NGC 4286 could be associated with a past interaction between it and its giant elliptical neighbor (e.g. DuPrie & Schneider 1996). IC 3475 is only ~ 170 kpc from the projected center of the Virgo Cluster (Vigroux et al. 1986), apparently placing it well within the cluster core. Even if it is actually in front of Virgo, as indicated by the recent distant estimates of Garcia et al. (1996), it is still apparently a member of a group with massive ellipticals. Thus, the evolution of all three galaxies may have been affected by their local environments.

The evolutionary history of these galaxies remains obscure. Additional information may be provided by the kinematics of the gas and the metallicities of the galaxies. By simultaneously determining the chemical enrichment of the ionized gas and studying the gas kinematics, we may be able to resolve these issues. Under the auspices of the “transition from dIm to dE/dS0” theory, one would expect that high atomic gas-to-light ratio galaxies in a pre-starburst phase would have lower abundances and relatively undisturbed gas kinematics, while galaxies that have just begun the starburst process would also have lower abundances and kinematical signatures of active star formation and supernovae-driven

winds. Dwarfs that have progressed further along the transition phase may show more chemical enrichment, lower atomic gas-to-light ratios, and a kinematical signature of supernovae-driven winds. Galaxies that have entered the postburst phase should also be chemically enriched, but no longer show signs of ongoing massive star formation. Abundance and kinematical information are necessary to determine if this scenario holds under scrutiny and whether it depends upon environmental considerations. If the kinematics and chemical abundances of NGC 3377A are consistent with the idea that it is in an earlier, less enriched, stage of development compared to NGC 4286, and the kinematics of NGC 4286 are consistent with gas loss through stripping or supernova driven winds, then we will have a indication that this hypothesis is valid. The relation of IC 3475 to other dwarf galaxies remains unclear, however. In order to examine this, we plan to obtain high resolution spectroscopy of the galaxies studied here.

4. Conclusions

We have examined the galaxies NGC 3377A, NGC 4286, and IC 3475 in B , R , and $H\alpha$. NGC 3377A is actively forming stars over most of its optical area, but at a very low level. It is quite gas-rich, and appears to be a dwarf spiral. If all of its gas is available to form stars, it can continue to maintain its current star formation level for much longer than a Hubble time, and this, along with its $B - R$ colors, argue against it evolving into an IC 3475-type galaxy in the near future. It may be a precursor to a galaxy resembling NGC 4286, but whether it can *physically* evolve into such a galaxy later in its evolution is unclear without further observations. NGC 4286 is a dwarf that may have lost most of its gas very recently, perhaps through stripping, or through supernovae-driven winds as it underwent an environmentally-induced episode of star formation. All of its current star formation is located in the inner half of the optical disk. At its current low SFR, however,

like NGC 3377A, it can continue to form stars for more than a Hubble time. Furthermore, its $B - R$ color is also inconsistent with the suggestion that it may evolve into a galaxy resembling IC 3475. IC 3475 appears to be a quiescent, gas-poor, low surface brightness galaxy, with no signs of ongoing or recent star formation activity. However, it is *too blue* to be a dE, and no obvious local counterpart to its precursor has yet been identified. Thus the evolutionary progression of these dwarf galaxies remains uncertain, and we find that using optical morphology, even when combined with some knowledge of the neutral gas content of a dwarf galaxy, is *not* sufficient to determine a galaxy’s evolutionary phase.

Other studies of “transition” dwarf galaxies reach similar conclusions that knowledge of optical morphology is not sufficient to constrain the evolutionary phase of dwarfs. For example, Sandage & Fomalont (1993) suggested based on red and yellow images, that the galaxy ESO 359-029 is a “transition dwarf” very similar to NGC 4286. Based on the photometry of Lauberts & Valentijn (1989), they derive $(B - R)_T = 0.63$, which is quite blue. Their follow-up H I observations, however, indicated that this galaxy is *not* gas poor, like NGC 4286, for which they derive $M_{HI}/L_B = 0.21$. This value is much closer to NGC 3377A than NGC 4286. Sandage & Fomalont then concluded that ESO 359-029 is a “transition dwarf” *between* the stages of NGC 3377A and NGC 4286. In fact, recent CCD observations of ESO 359-029 show this galaxy to have the morphology of an extreme late-type Sd spiral (Matthews & Gallagher 1997). Furthermore, Matthews & Gallagher derive moderately red optical colors, $(B - V)_T = 0.62$, at odds with the blue colors found by Sandage & Fomalont. Also, despite moderately red colors, H II regions and diffuse emission from ionized gas are also seen in a long slit spectrum (Matthews 1998), while high signal-to-noise pencil beam H I observations show a normal line profile and $M_{HI}/L_V = 0.43$ (Matthews et al. 1998). This system is neither gas-poor, like NGC 4286, nor a drop out from star-forming activity, like NGC 3377A. Given the conflicting results for the optical colors, it also remains unclear whether this galaxy, even if it lies between the evolutionary

stages of NGC 3377A and NGC 4286, as suggested by Sandage & Fomalont, could ever evolve into a galaxy like IC 3475.

Obviously, in order to truly begin to deconvolve the evolution of dwarf galaxies, a statistically significant sample needs to be studied. This sample needs to be selected to distinguish between environmental and internal effects. Furthermore, information about the kinematics of the gas and the metallicities of the galaxies is also needed to disentangle the different possible evolutionary paths. The study presented here represents the first step in an ongoing project to accomplish these goals.

The H α filter set used for this research was kindly loaned to us by Deidre Hunter. Rosa Gonzalez provided us with the scripts for the spectrophotometric data reduction, Ricky Patterson offered many helpful comments on the surface photometry, and Gerhardt Meurer provided helpful discussions. In addition, we would like to thank the staff at the Michigan-Dartmouth-MIT Observatory for their assistance and support in this project. PMK and KRS acknowledge support from NASA Long Term Space Astrophysics grant NAG5-3485. JSG wishes to thank the National Science Foundation for partial support of his research on dwarf galaxies through grant NSF AST-9803018.

REFERENCES

- Bender, R. & Nieto, J.L. 1990, *A&A*, 239, 97
- Babul, A. & Rees, M. J. 1992, *MNRAS*, 255, 346
- Binggeli, B. 1986, in *Star Forming Dwarfs and Related Objects*, eds. D. Kunth, T. X. Thuan, J. T. T. Thuan (Gif sur Yvette: Editions Frontières), p52
- Bothun, G. D., Aaronson, M., Schommer, B., Mould, J., Huchra, J., & Sullivan, W. T., III 1985, *ApJS*, 57, 423
- Bothun, G. D., Mould, J. R., Caldwell, N., & MacGillivray, H. T. 1986, *AJ*, 92, 1007
- de Blok, W. J. G., van der Hulst, J. M., & Bothun, G. D. 1995, *MNRAS*, 283, 18
- De Young, D. & Heckman, T. F. 1994, *ApJ*, 431, 598
- de Vaucouleurs, G. 1959, in *Handbuch der Physik*, v. 53, *Astrophysics IV: Stellar Systems*, ed. S. Flügge (Berlin: Springer-Verlag), p275
- de Vaucouleurs, G., de Vaucouleurs, A., Corwin, H. G., Buta, R., Paturel, G., & Fouqué, P. 1991, *Third Reference Catalogue of Bright Galaxies* (Springer, New York) (RC3)
- Dekel, A. & Silk, J. 1986, *ApJ*, 303, 39
- Diplas, A. & Savage, B. D. 1994, *ApJ*, 427, 274
- DuPrie, K. & Schneider, S. E. 1996, *AJ*, 112, 937
- Faber, S. & Lin, D. 1983, *ApJ*, 266, 21
- Ferguson, H. C. & Binggeli, B. 1994, *ARA&A*, 6, 67
- Gallagher, III, J. S. & Hunter, D. A. 1986, *AJ*, 92, 557

- Gallagher, III, J. S. & Hunter, D. A. 1989, *AJ*, 98, 806
- Gallagher, III, J. S. & Wyse, R. F. G. 1994, *PASP*, 106, 1225
- Garcia, A. M., Fournier, H. di Nella, & Paturel, G. 1996, *A&A*, 310, 412
- Gardiner, L. T. & Noguchi, M. 1996, *MNRAS*, 278, 191
- Gerin, M. & Casoli, F. 1994, *A&A*, 290, 49
- Gruendl, R. A., Vogel, S. N., Davis, D. S., & Mulchaey, J. S. 1993, *ApJ*, 413, L81
- Hartmann, D. & Burton, W. B. 1997, *Atlas of Galactic Neutral Hydrogen*, (Cambridge: Cambridge University Press)
- Henriksen, M. & Byrd, G. 1996, *ApJ*, 459, 82
- Huchtmeier, W. K. & Richter, O. G. 1986, *A&AS*, 64, 111
- Hunter, D. A. & Gallagher, III, J. S. 1985, *ApJS*, 58, 533
- Kennicutt, Jr., R. C. & Hodge, P. W. 1986, *ApJ*, 306, 130
- Kennicutt, Jr., R. C., Tamblyn, P., & Congdon, C. W. 1994, *ApJ*, 432, 22
- Kennicutt, Jr., R. C., Freedman, W. L., & Mould, J. R. 1995, *AJ*, 110, 1476
- Knezek, P. M. 1993, Ph. D. Thesis, University of Massachusetts
- Kormendy, J. 1985, *ApJ*, 295, 73
- Landolt, A. U. 1992, *AJ*, 104, 340
- Lauberts, A. & Valentijn, E. A. 1989, *Surface Photometry Catalog of the ESO-Uppsala Galaxies:ESO*

- Lin, D. N. C. & Faber, S. M. 1983, *ApJ*, 266, 21
- Marconi, G., Matteucci, F., & Tosi, M. 1994, *MNRAS*, 270, 35
- Matteucci, F., & Chiosi, C. 1983, *A&A*, 123, 121
- Matteucci, F., & Tosi, M. 1985, *MNRAS*, 217, 391
- Matthews, L. D. 1998, Ph.D. thesis, State University of New York at Stony Brook
- Matthews, L. D. & Gallagher, III, J. S. 1997, *AJ*, 114, 1899
- Matthews, L. D., van Driel, W., & Gallagher, III, J. S. 1998, *AJ*, in press
- McGaugh, S. S. & Bothun, G. D. 1994, *AJ*, 107, 530
- McGlynn, T. A. & Borne, K. D. 1991, *ApJ*, 372, 31
- Moore, B., Lake, G., & Katz, N. 1998, *ApJ*, 495, 139
- Moore, B., Katz, N., & Lake, G. 1996, *ApJ*, 457, 455
- Noguchi, M. 1988, *A&A*, 201, 37
- Oh, K. S., Lin, D. N. C., & Aarseth, S. J. 1995, *ApJ*, 442, 1420
- Oke, J. B. & Gunn, J. E. 1983, *ApJ*, 266, 713
- Pilyugin, L. S. 1992, *A&A*, 260, 58
- Pilyugin, L. S. 1993, *A&A*, 277, 42
- Reaves, G. 1956, *AJ*, 61, 69
- Reed, B. C. 1985, *PASP*, 97, 120
- Sandage, A. 1965, *ApJ*, 141, 1560

- Sandage, A., & Binggeli, B. 1984, *AJ*, 89, 919
- Sandage, A., & Fomalont, E. 1993, *ApJ*, 407, 14
- Sandage, A., & Hoffman, G. L. 1991, *ApJ*, 379, 45
- Schaller, G., Schaerer, D., Meynet, G., & Maeder, A. 1993, *A&AS*, 96, 269
- Schombert, J. M., Bothun, G. D., Impey, C. D., & Mundy, L. G. 1990, *AJ*, 100, 1523
- Schombert, J. M., Pildis, R. A., Eder, J. A., & Oemler, Jr. A. 1995, *AJ*, 110, 2067
- Schneider, S. E., Thuan, T. X., Magri, C., & Wadiak, J. E. 1990, *ApJS*, 72, 245
- Searle, L. & Zinn, R. 1978, *ApJ*, 225, 357
- Secker, J., Harris, W. E., & Plummer, J. D. 1997, *PASP*, 109, 1377
- Séguin, P. & Dupraz, C. 1996, *A&A*, 310, 757
- Silk, J., Wyse, R. F. G., & Shields, G. A. 1987, *ApJ*, 322, L59
- Silk, J. & Wyse, R. F. G. 1993, *Phys. Rep.*, 231, 293
- Skillman, E. D. & Bender, R. 1995, *RevMexAASC*, 3, 25
- Sofue, Y. 1994, *ApJ*, 423, 207
- Spaans, M. & Norman, C. 1997, *ApJ*, 483, 87
- Strong, A. W., Bloemen, J. B. G. M., Dame, T. M., Grenier, I. A., Hermsen, W., Lebrun, F., Nyman, L.-A., Pollock, A. M. T., Thaddeus, P. 1988, *A&A*, 207, 1
- Thuan, T. X. 1985, *ApJ*, 299, 881
- Tonry, J. L., Blakeslee, J. P., Ajhar, E. A., & Dressler, A. 1997, *ApJ*, 475, 399.

Valluri, M. 1993, *ApJ*, 408, 57

van Zee, L., Haynes, M. P., Salzer, J. J., & Broeils, A. H. 1996, *AJ*, 112, 129

van Zee, L., Haynes, M. P., & Salzer, J. J. 1997, *AJ*, 114, 2479 (van Zee et al. 1997a)

van Zee, L., Haynes, M. P., & Salzer, J. J. 1997, *AJ*, 114, 2497 (van Zee et al. 1997b)

Vigroux, L., Thuan, T. X., Vader, J. P., & Lachieze-Rey, M. 1986, *AJ*, 91, 70

Walsh, J. R., Dudziak, G., Minniti, D., Zilstra, A. A. 1997, *ApJ*, 487, 651

Wilson, C. D. 1995, *ApJ*, 448, 97

Windhorst, R. A. et al. 1991, *ApJ*, 380, 362

Wirth, A. & Gallagher, III, J. S. 1984, *ApJ*, 282, 85

Young, J. S., & Knezek, P. M. 1989, *ApJ*, 347, 55

Fig. 1a.— The image shows a greyscale $4.2' \times 4.2'$ B -band image of NGC 3377A. A bar representing $15''$ is in the lower right corner. North and east are indicated.

Fig. 1b.— The image is a $4.2' \times 4.2'$ three-color image of NGC 3377A. Blue represents B -band, red represents R -band, and green represents the continuum-subtracted $H\alpha$ emission. Colors have been determined to maximize contrast. North and east are indicated.

Fig. 1c.— The image shows a greyscale $4.2' \times 4.2'$ B -band image of NGC 4286. A bar representing $15''$ is in the lower right corner. North and east are indicated.

Fig. 1d.— The image is a $4.2' \times 4.2'$ three-color image of NGC 4286. Blue represents B -band, red represents R -band, and green represents the continuum-subtracted $H\alpha$ emission. Colors have been determined to maximize contrast. North and east are indicated.

Fig. 1e.— The image shows a greyscale $4.2' \times 4.2'$ B -band image of IC 3475. A bar representing $15''$ is in the lower right corner. North and east are indicated.

Fig. 1f.— The image is a $4.2' \times 4.2'$ three-color image of IC 3475. Blue represents B -band, red represents R -band, and green represents the continuum-subtracted $H\alpha$ emission. Colors have been determined to maximize contrast. North and east are indicated.

Fig. 2a.— The upper panel shows the B (filled squares), R (filled circles), and $H\alpha$ (filled triangles) surface brightnesses as a function of radius for NGC 3377A. The dashed lines are the best fit to a line using only the data at $r > 60''$ in B and R . The middle panel shows the integrated $B - R$ color as a function of radius within $5''$ annuli. The bottom panel shows the annular $B - R$ color as a function of radius within $5''$ annuli.

Fig. 2b.— The upper panel shows the B (filled squares), R (filled circles), and $H\alpha$ (filled triangles) surface brightnesses as a function of radius for NGC 4286 along the major axis. The dashed lines are the best fit to a line using only the data at $r > 60''$ in B and R . The

middle panel shows the integrated $B - R$ color as a function of radius within $5''$ annuli. The bottom panel shows the annular $B - R$ color as a function of radius within $5''$ annuli.

Fig. 2c.— The upper panel shows the B (filled squares), R (filled circles), and $H\alpha$ (filled triangles) surface brightnesses as a function of radius for IC 3475. The $H\alpha$ surface brightnesses are 3σ upper limits. The dashed lines are the best fit to a line using only the data at $r > 60''$ in B and R . The middle panel shows the integrated $B - R$ color as a function of radius within $5''$ annuli. The bottom panel shows the annular $B - R$ color as a function of radius within $5''$ annuli.

This figure "f1a.jpg" is available in "jpg" format from:

<http://arxiv.org/ps/astro-ph/9810119v1>

This figure "f1b.jpg" is available in "jpg" format from:

<http://arxiv.org/ps/astro-ph/9810119v1>

This figure "f1c.jpg" is available in "jpg" format from:

<http://arxiv.org/ps/astro-ph/9810119v1>

This figure "f1d.jpg" is available in "jpg" format from:

<http://arxiv.org/ps/astro-ph/9810119v1>

This figure "fle.jpg" is available in "jpg" format from:

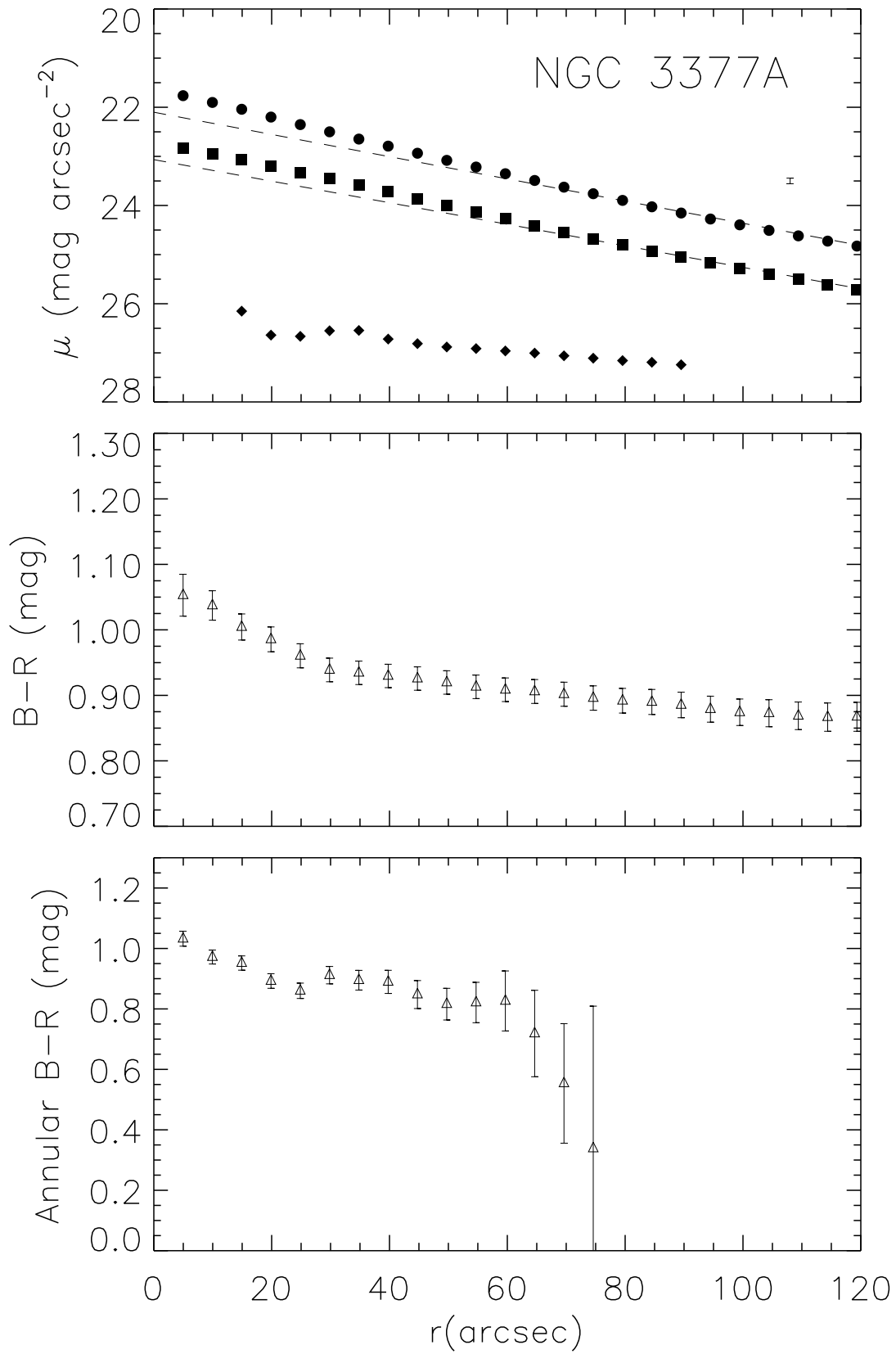
<http://arxiv.org/ps/astro-ph/9810119v1>

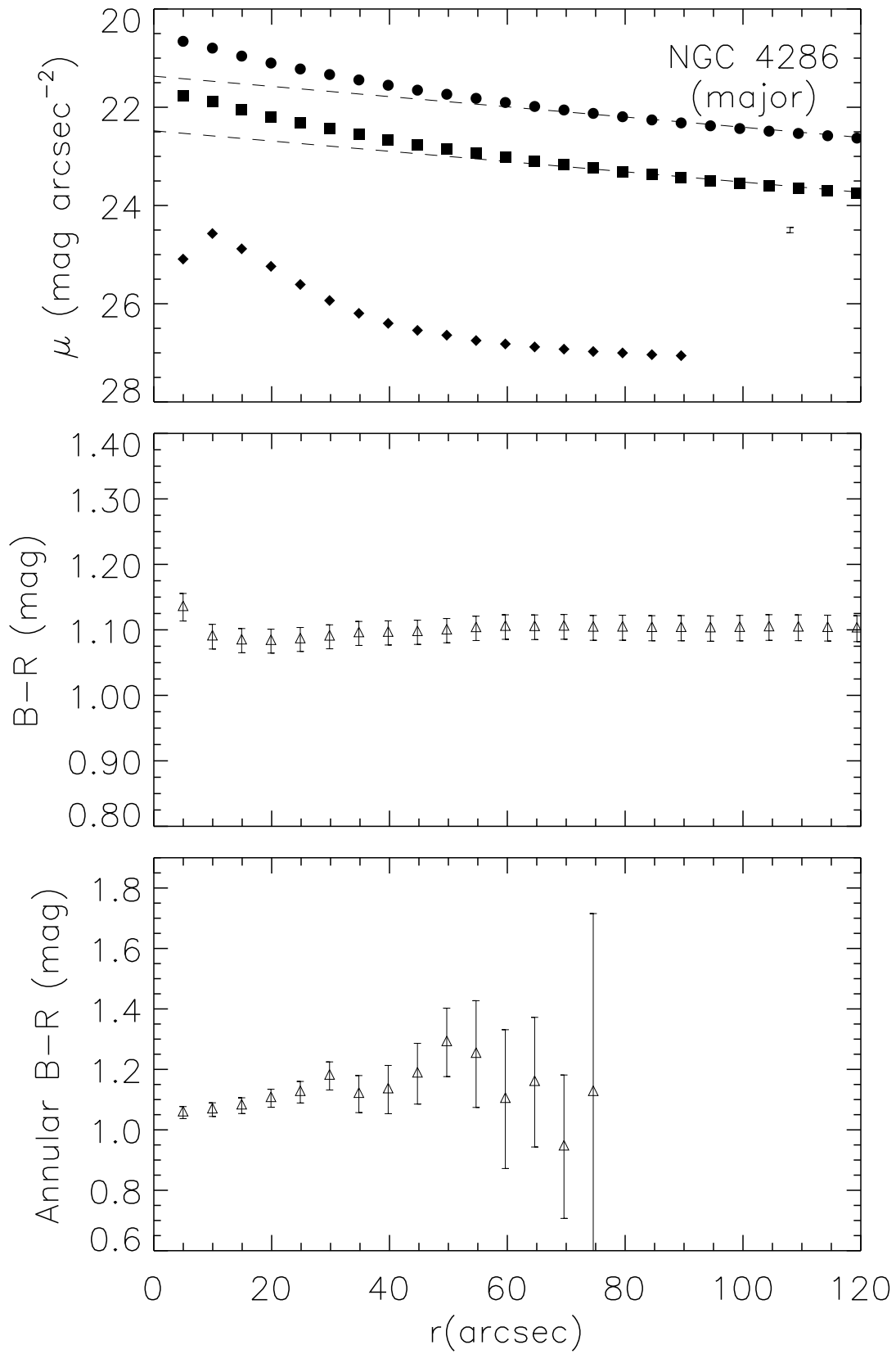
This figure "f1f.jpg" is available in "jpg" format from:

<http://arxiv.org/ps/astro-ph/9810119v1>

TABLE 1
 CATALOGED PROPERTIES OF THE DWARF “TRANSITION” GALAXIES

Galaxy	α (J2000) h m s	δ (J2000) ° ′ ″	v_{helio} km sec ⁻¹	a ′	b ′	B_T	S_{HI} Jy km s ⁻¹	Morphological Type
NGC 3377A	10:47:23.0	+14:04:03	572	2.2	2.1	14.22	5.21	SAB(s)m
NGC 4286	12:20:41.9	+29:20:45	644	1.6	1.0	...	0.67	SA(r)0/a:
IC 3475	12:32:40.8	+12:46:13	2583	1.7	1.6	13.82	<1.50	E:





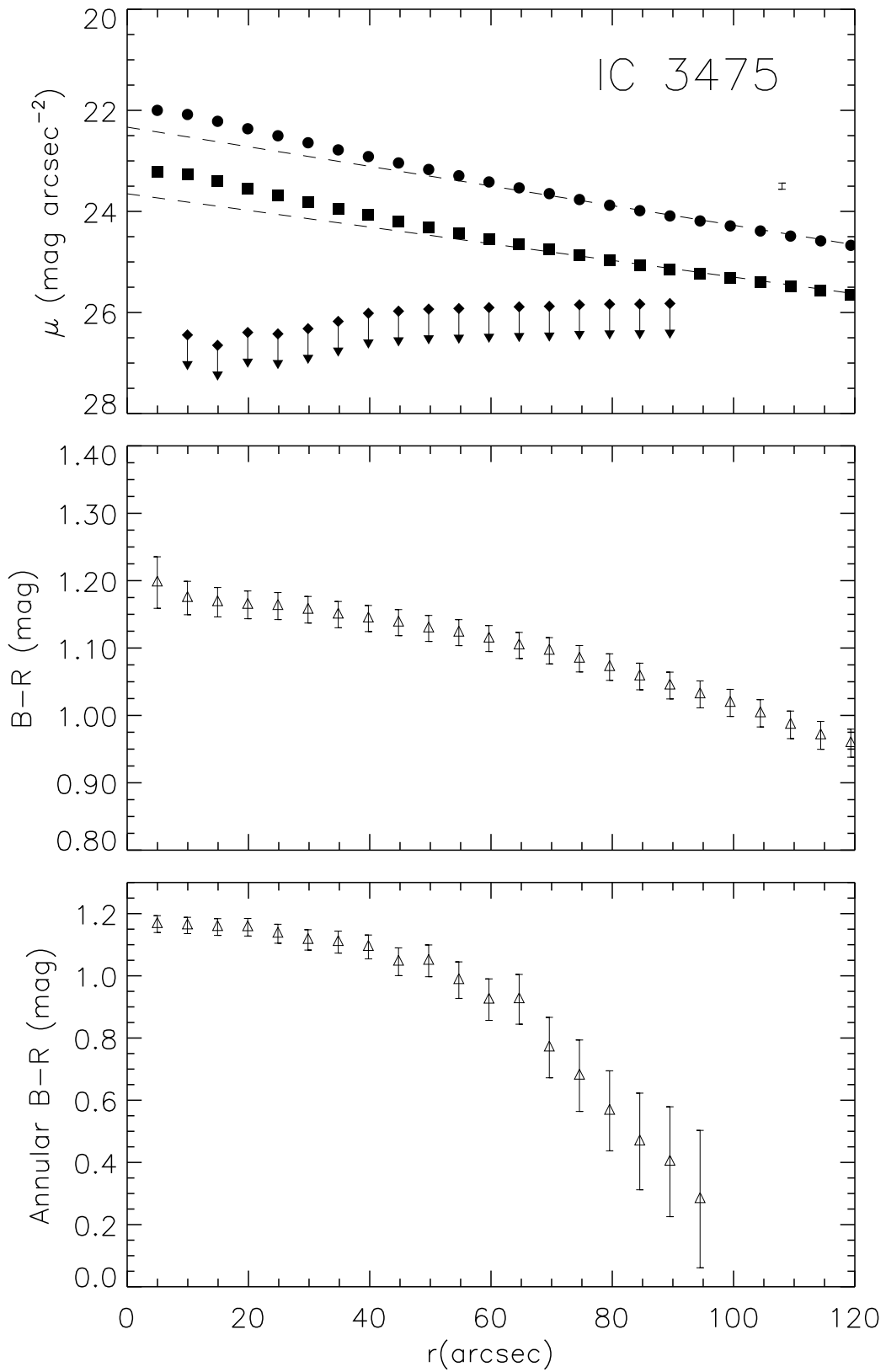


TABLE 2
PHOTOMETRY OF THE DWARF “TRANSITION” GALAXIES

Galaxy	m_B	m_R	$m_{H\alpha}$ ^a	$m_B - m_R$	$D(B_{25})$ /'	$E(B - V)$
NGC 3377A	14.20 ± 0.05	13.04 ± 0.05	$16.58^{+0.40}_{-0.29}$	1.15 ± 0.04	1.47	0.06
NGC 4286	13.71 ± 0.05	12.44 ± 0.04	$17.32^{+0.38}_{-0.29}$	1.26 ± 0.03	1.63	0.05
IC 3475	13.95 ± 0.05	12.83 ± 0.05	$\gtrsim 15.30$	1.10 ± 0.04	1.36	0.04

^aSee text for an explanation of the $H\alpha$ errors.

TABLE 3
 DERIVED PROPERTIES OF THE DWARF “TRANSITION” GALAXIES

Galaxy	D Mpc	M_B	M_R	$L_{H\alpha}$ $10^{38} \text{ erg s}^{-1}$	M_{HI} $10^7 M_\odot$	M_{H2} $10^7 M_\odot$	M_{HI}/L_B	SFR $10^{-3} M_\odot \text{ yr}^{-1}$	Log (M_{HI}/SFR)
NGC 3377A	10.7	-16.20	-17.22	2.6	14.1	...	0.30	3.3	10.78
NGC 4286	15.5	-17.44	-18.62	2.7	3.8	1.1	0.03	3.4	10.21
IC 3475	14.2	-16.81	-17.93	$\lesssim 12.0$	< 7.1	...	$\lesssim 0.09$	$\lesssim 15.1$...

TABLE 4
 LINEAR FITS TO $R_{\gtrsim 60''}$

Galaxy	Filter	μ_0 mag arcsec $^{-2}$	α arcsec	α kpc
NGC 3377A	<i>B</i>	23.07	49.6	2.57
	<i>R</i>	22.10	48.1	2.49
NGC 4286	<i>B</i>	23.04	54.3	4.08
	<i>R</i>	21.87	52.2	3.92
IC 3475	<i>B</i>	23.65	65.8	4.55
	<i>R</i>	22.33	60.0	3.85